Nature of the magnetic interactions in Sr_3NiIrO_6

Turan Birol
Department of Physics and Astronomy, Rutgers University, Piscataway, New Jersey 08854, USA
and Department of Chemical Engineering and Materials Science, University of Minnesota, Minneapolis, Minnesota 55455, USA

Kristjan Haule and David Vanderbilt
Department of Physics and Astronomy, Rutgers University, Piscataway, New Jersey 08854, USA

(Received 27 April 2018; revised manuscript received 14 August 2018; published 18 October 2018)

Iridates abound with interesting magnetic behaviors because of their strong spin-orbit coupling. Sr_3NiIrO_6 brings together the spin-orbital entanglement of the Ir^{4+} ion with a 3*d* Ni cation and a one-dimensional crystal structure. It has a ferrimagnetic ground state with a 55-T coercive field. We perform a theoretical study of the magnetic interactions in this compound, and elucidate the role of anisotropic symmetric exchange as the source of its strong magnetic anisotropy. Our first-principles calculations reproduce the magnon spectra of this compound and predict a signature in the cross sections that can differentiate the anisotropic exchange from single-ion anisotropy.

DOI: 10.1103/PhysRevB.98.134432

I. INTRODUCTION

Oxides of 5*d* transition metals, especially iridates, are at the center of recent interest because of their strong spin-orbit coupling (SOC) [1,2]. SOC gives rise to phenomena such as anisotropic pseudodipolar magnetic exchange interactions [3]. These interactions in turn lead to phases such as the quantum spin liquid in the Kitaev model, which might be realized in honeycomb iridates [4].

The magnetic behavior of complex oxides with multiple inequivalent transition-metal cations can also be very rich, especially when the transition metals come from different rows of the periodic table. For example, the 3*d*-5*d* double perovskites are known to display incommensurate antiferromagnetism, multiferroicity, magnetoresistance, half-metallic ferrimagnetism, independent ordering of interpenetrating magnetic lattices, and very often high ordering temperatures [5–9]. Interesting phenomena are still being discovered in these systems, such as the recent demonstration of magnetic interactions in Ca_2CoOsO_6 and Ca_2NiOsO_6 that break the Goodenough-Kanamori-Anderson (GKA) rules [10].

Another structural family of compounds that contain two different transition-metal cations is the $A_3MM'O_6$ chain compounds with the K_4CdCl_6 crystal structure [11]. Many members of this family exhibit phenomena such as multiferroicity, unexpectedly strong magnetic anisotropy, colossal magnon gaps, superparamagneticlike behavior, and partially disordered antiferromagnetism [12–17]. Ferrimagnetic Sr_3NiIrO_6 [18], a member of this family, displays Ising-like magnetic anisotropy, a record-breaking magnetic coercive field [19], and a colossal spin-wave gap [20,21]. All of these are surprising observations because neither Ni^{2+} nor Ir^{4+} should have strong single-ion magnetic anisotropy (SIA).

In this work, we approach the magnetic interactions in Sr_3NiIrO_6 from first principles and elucidate the microscopic mechanism behind its magnetism. Our main result is that the effective magnetic interaction between nearest-neighbor ions' moments $\mathbf{M}_i$ is symmetric but *radically anisotropic*. In other words, while the energy expression does not contain antisymmetric cross product terms, it has opposite signs for different components of the magnetic moments. This radically anisotropic symmetric interaction can be written as

$$E = J_{\parallel} M_{i,z} M_{i+1,z} + J_{\perp}(M_{i,x} M_{i+1,x} + M_{i,y} M_{i+1,y}), \quad (1)$$

where $J_{\parallel}$ and $J_{\perp}$ have opposite signs. The strong Ising-like behavior observed in this compound can be explained by this energy expression without a single-ion anisotropy (SIA) term. We reproduce all three important qualitative aspects of the experimental magnon spectra (a small bandwidth, a much larger splitting of the bands, and a gap comparable to the splitting of magnon branches) [20,21], using this model with parameters fitted to first-principles calculations without any fine tuning of parameters. We predict that a corollary of the radically anisotropic exchange is the flipping of the oscillation patterns of optical and acoustic magnons at the Γ point, and conclude by putting forward a signature in the magnon-creation neutron-scattering cross sections that can be used to experimentally differentiate between the anisotropic exchange scenario and the commonly used isotropic exchange with strong SIA.

Sr_3NiIrO_6 has been previously studied theoretically by multiple authors, starting with Vajenine and Hoffmann's Hueckel calculations [22]. Zhang *et al.*, using density functional theory (DFT), underlined the importance of the SOC, and reported considerable orbital moments for both transition metals [23]. Sarkar *et al.* verified the presence of large orbital moments [24]. Ou and Wu pointed out the importance of SOC in altering the orbital configuration of Ir, and found that it is responsible for the intrachain ferrimagnetic order [25]. Most recently, Gordon *et al.* elucidated a connection between the magnetic exchange interactions and the Ising behavior in

 ©2018 American Physical Society

Sr_3NiIrO_6 [26]. Our work goes beyond these first-principles calculations, and in addition to explaining the microscopic mechanism of the anisotropic exchange interaction in this $3d$-$5d$ system, bridges the gap between the first-principles calculations and experimental observations by calculating the magnetic interaction parameters from first principles and reproducing the experimentally observed magnon spectra.

II. MAGNETIC STRUCTURE

The structure of Sr_3NiIrO_6 consists of parallel one-dimensional chains of alternating face-sharing NiO_6 and IrO_6 polyhedra as shown in Fig. 1(a) [11,18]. There are two different energy scales for magnetic couplings along the c axis (intrachain) and in the ab plane (interchain). Similarly, there are two temperature scales for magnetism. At T_2, intrachain magnetic order sets in. The temperature scale for the interchain magnetic order, T_1, is usually about an order of magnitude smaller than T_2. This is because there are no good superexchange paths that connect magnetic moments in different chains, but also because the chains form a frustrated triangular lattice. In Sr_3NiIrO_6, $T_2 = 75$ K, and the intrachain order is ferrimagnetic: both the Ni and Ir moments are aligned along the c axis (chain direction), but are antiparallel to each other [27]. The interchain order below $T_1 = 17$ K is still under debate: neutron data are consistent with both the so-called partially disordered and the amplitude-modulated antiferromagnetic arrangements of the ferrimagnetic chains [27]. In this work, we focus only on the intrachain interactions, and do not address the question of interchain magnetic order.

In Fig. 2(a) we plot the energy-resolved density of states on the Ir ion, with the projections on the $|3z^2 - r^2\rangle$ orbital plotted separately, from DFT+U+SOC calculations. In our choice of coordinate axes, shown in Fig. 1(b), the $|3z^2 - r^2\rangle$ orbital of Ir has t_{2g}-like character with lobes extended towards the nearest-neighbor Ni ions as shown in Fig. 1(c). This makes it the most important orbital for the superexchange interactions [28]. The Ir^{4+} cation has five d electrons in its valence shell. Its unoccupied e_g states lie between 3 and 4 eV (not shown), and it has a single Ir t_{2g} hole between 0.5 and 1.0 eV. This hole has 36% $|3z^2 - r^2\rangle$ character, and a nontrivial spin

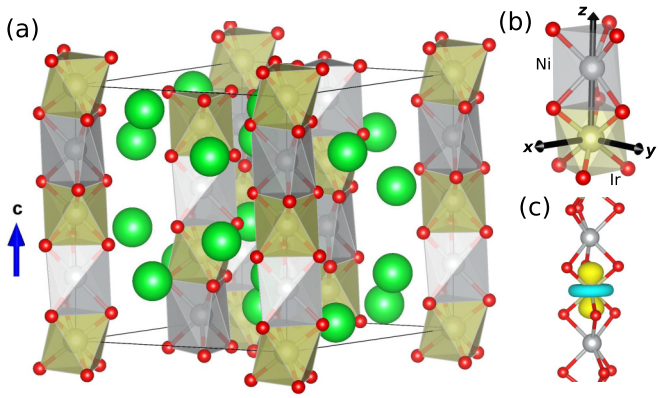

FIG. 1. (a) Crystal structure of Sr_3NiIrO_6. Green, grey, yellow, and red spheres represent Sr, Ni, Ir, and O ions respectively. (b) The local axes used for the Ir ions. (c) The $|3z^2 - r^2\rangle$ orbital on an Ir ion.

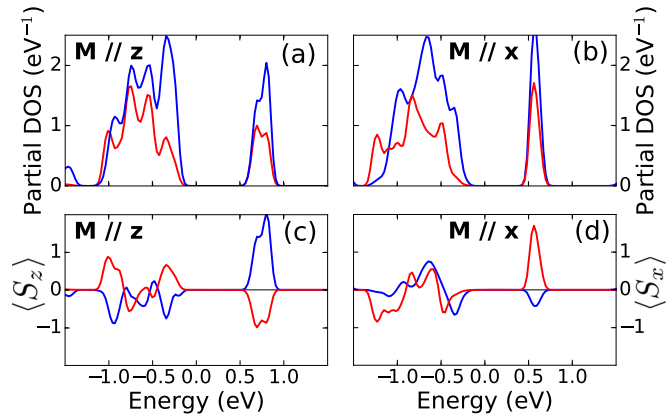

FIG. 2. (a) Densities of states of the Ir ion projected onto the d orbitals in the FiM state with magnetic moments along the z axis (magnetic ground state). Red curve is the DOS projected onto the $|3z^2 - r^2\rangle$ orbital, and the blue curve is the sum of the projected DOS's onto the other four d orbitals. (b) Same quantity as in (a), but in the FM state with magnetic moments along the x axis. (c) Energy resolved expectation value of the z component of spin $\langle S_z \rangle$ for the d orbitals of the Ir ion in the FiM state with magnetic moments along the z axis. (d) Same quantity as in (c), but in the FM state with magnetic moments along the x axis.

characteristic: its $|3z^2 - r^2\rangle$ contribution has the opposite spin relative to the rest of the hole, as seen in the energy-resolved spin expectation value $\langle S_z \rangle$ in Fig. 2(c). This can be explained by the strong SOC of the Ir ion: the hole on the Ir does not have a definite spin, but it has $J_{\text{eff}} = 1/2$ character and can be thought to have a corresponding *pseudospin*. The $J_{\text{eff}} = 1/2$ orbitals with pseudospin in the $\mp\hat{z}$ directions are

$$|J_{1/2}, \uparrow\rangle = \frac{1}{\sqrt{|\gamma|^2 + 2}}(i\gamma|A, \downarrow\rangle + \sqrt{2}|E^+, \uparrow\rangle) \quad (2)$$

and

$$|J_{1/2}, \downarrow\rangle = \frac{1}{\sqrt{|\gamma|^2 + 2}}(i\gamma|A, \uparrow\rangle + \sqrt{2}|E^-, \downarrow\rangle), \quad (3)$$

where $|A\rangle = |3z^2 - r^2\rangle$ and $|E^{\mp}\rangle$ are the t_{2g}-like orbitals that are split by the trigonal field (in the absence of the trigonal crystal field, $\gamma = 1$). As a result, *the spin moment on the* $|A\rangle = |3z^2 - r^2\rangle$ *orbital is opposite to the total spin moment (as well as the pseudospin moment) of the Ir ion when it is along the z direction.*

III. MAGNETIC INTERACTIONS

The effective magnetic Hamiltonian for the Ir ion with an electron in the $J_{\text{eff}} = 1/2$ orbital needs to be built using not the spin, but rather the pseudospin of the electron. The SOC reduces the orbital degeneracy in iridates, but the magnetic Hamiltonians are usually more complicated and may involve anisotropic exchange interactions which couple different components of pseudospins with different strengths [3,29]. Anisotropic exchange interactions can set a preferred axis for the pseudospin moments and give rise to other effects that are usually ascribed to SIA. For example, the magnon gap

observed in $Sr_3Ir_2O_7$ is explained by the exchange anisotropy between the Ir^{4+} ions [30].

The GKA rules [31] for the signs of the exchange interactions do not directly apply to the pseudospins since the orbital degree of freedom is entangled with spin [10]. Instead, we need to consider the individual orbital components of the $J_{\rm eff} = 1/2$ spin orbitals and the interactions between them. A tight-binding model constructed using the *ab initio* Wannier functions [32,33] that only includes the Ni d and Ir t_{2g} orbitals shows that the largest hopping is between the $|A\rangle$ orbital on the Ir and the similar $|3z^2 - r^2\rangle$ on the Ni as expected in this face-sharing polyhedral geometry.

The DOS projected onto Ni shows [28] that the $|3z^2 - r^2\rangle$ orbital on Ni^{2+} is fully occupied. The superexchange process in which a Ni electron is excited to an Ir $|A\rangle$ orbital is possible only if the electron has opposite spin to the spin on the Ir $|A\rangle$ orbital, and provides an energy gain proportional to the Ni on-site Hund's coupling if the Ni spin is parallel to that on the Ir $|A\rangle$ orbital [31]. This implies that there is a ferromagnetic coupling between the Ni spin and the spin on the Ir $|A\rangle$ orbital. Since the total spin expectation value $\langle S_z\rangle$ of the Ir ion is opposite to the spin on the Ir $|A\rangle$ orbital, this superexchange provides an antiferromagnetic (ferrimagnetic) coupling between the total magnetic moments of the Ni and the Ir ions. The inclusion of other orbitals in this argument [28] does not change the sign of this coupling, which explains the ferrimagnetic ground state observed in Sr_3NiIrO_6.

In our picture, then, this antiferromagnetic interaction, which emerges from a ferromagnetic superexchange, is a direct result of the strong SOC on the Ir ion. In order to test this claim further, we repeated a similar DFT calculation with SOC turned off, and could stabilize only the FM configuration. This is consistent with Ref. [24] where SOC was not taken into account and consequently only the FM order was stabilized. A similar point about different orbitals contributing to superexchange in a nontrivial way due to SOC is also made in Ref. [13], where a ferromagnetic exchange anisotropy stemming from an antiferromagnetic exchange interaction in Sr_3CuIrO_6 is studied.

The Ir $|A\rangle$ orbital has opposite spin to that of the $|E^{\mp}\rangle$ orbitals only when the Ir pseudospin is along $\hat{z}$. If the Ir magnetic moment is in another direction, this condition will no longer be satisfied. For example, the $J_{\rm eff} = 1/2$ state with pseudospin parallel to $\hat{x}$,

$$|J_{1/2}, \uparrow_x\rangle = (|J_{1/2}, \uparrow\rangle + |J_{1/2}, \downarrow\rangle)/\sqrt{2}, \tag{4}$$

has the form

$$|J_{1/2}, \uparrow_x\rangle = (i\gamma\sqrt{2}|A, \uparrow_x\rangle + |E^+, \uparrow_x\rangle + |E^-, \uparrow_x\rangle + |E^+, \downarrow_x\rangle - |E^-, \downarrow_x\rangle)/\sqrt{2(|\gamma|^2 + 2)}, \tag{5}$$

where $|\uparrow_x\rangle = (|\uparrow\rangle + |\downarrow\rangle)/\sqrt{2}$ and $|\downarrow_x\rangle = (|\uparrow\rangle - |\downarrow\rangle)/\sqrt{2}$. The spin on the $|A\rangle$ orbital is now parallel to the pseudospin of the $|J_{\rm eff}, \uparrow_x\rangle$ orbital. DFT results with the spins aligned in the x-y plane, shown in Figs. 2(c) and 2(d), are consistent with this observation: the $\langle S_x\rangle$ of the hole on $|A\rangle$ is parallel to the minority spin direction. In this case, the ferromagnetic superexchange between the Ni ion and the Ir $|A\rangle$ orbital should give rise to a ferromagnetic coupling between the magnetic moments of these ions. In other words, the effective interaction between the magnetic moments M on the nearest-neighbor Ni-Ir atoms is anisotropic and has the form $E = J_\parallel M_z^{\rm Ir} M_z^{\rm Ni} + J_\perp M_{xy}^{\rm Ir} M_{xy}^{\rm Ni}$ with $J_\parallel > 0$ but $J_\perp < 0$.

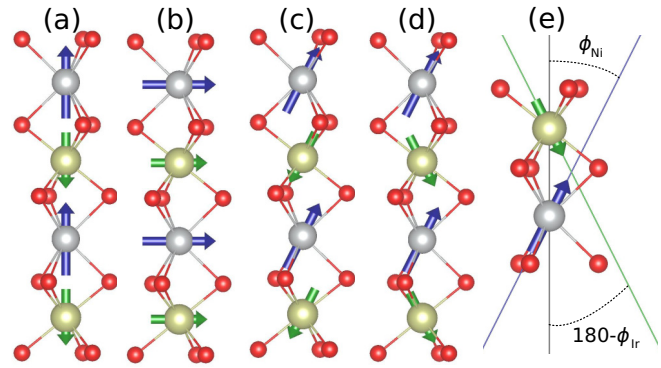

FIG. 3. (a) Ferrimagnetic state with moments along the z axis, which is the lowest-energy state (FiM-z: $\phi_{\text{Ni-Ir}} = 180°$, $\phi_{\rm Ni} = 0°$, $\phi_{\rm Ir} = 180°$). (b) Ferromagnetic state with moments along the x axis (FM-x: $\phi_{\text{Ni-Ir}} = 0°$, $\phi_{\rm Ni} = 90°$, $\phi_{\rm Ir} = 90°$). (c) Possible ferrimagnetic intermediate state ($\phi_{\text{Ni-Ir}} = 180°$). (d) Observed, canted ferrimagnetic intermediate state ($\phi_{\text{Ni-Ir}} < 180°$). (e) Definitions of $\phi_{\rm Ni}$ and $\phi_{\rm Ir}$.

DFT calculations provide estimates of $J_\perp$ and $J_\parallel$ that support this claim. We adopt the standard approach of initiating the DFT calculations in different magnetic configurations to estimate the energy differences between various magnetic states. However, especially in noncollinear calculations, it is not always possible to stabilize the system in the desired local energy minima if the system is very far from its ground state.[1] When we initiate our DFT calculation with spins parallel to $\hat{z}$, all of our calculations (even those initiated with FM order) converge to the ferrimagnetic configuration [FiM-z, Fig. 3(a)]. On the other hand, we could not stabilize a FiM state with spins in the x-y plane; the only state we could stabilize with moments in the x-y plane is the ferromagnetic one [FM-x, Fig. 3(b)].

To gain information about the magnetic interactions, then, we compute the energy at both of the energy minima [FM-x and FiM-z, shown in Figs. 3(a) and 3(b)], where it is possible to converge the electronic state to a very high precision, and also at several intermediate states where the magnetic moments are tilted. We do not observe any local minima in the vicinity of these intermediate states, but the slope of the electronic energy surface is so small (changing by less than about 10^{-5} eV/atom from one self-consistent iteration to the next) that we believe it is well justified to estimate the energy of these intermediate states in this way.[2]

We summarize our results in Fig. 4. The horizontal axis in these plots is the relative angle between the magnetic moments of Ir and Ni ions, $\phi_{\text{Ni-Ir}}$. In Figs. 4(a) and 4(b), we plot the total energy per formula unit, and in Fig. 4(c), we plot the angles $\phi_{\rm Ir}$ and $\phi_{\rm Ni}$ that the two magnetic moments make with the z axis [as defined in Fig. 3(e)]. There is a clear trend

[1] Some other studies (Refs. [23,25]) found similar behavior.

[2] Keeping the calculation running until self-consistency results in these intermediate states eventually converging to either FM-x or FiM-z.

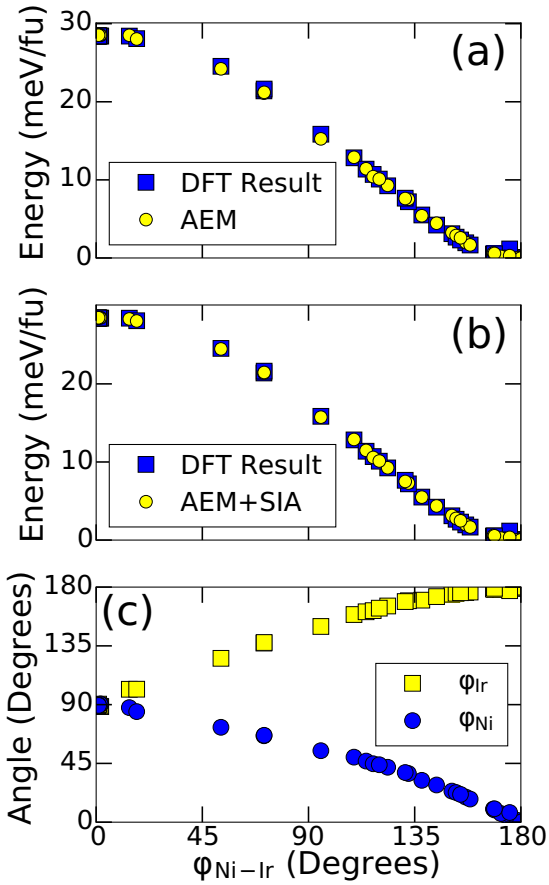

FIG. 4. First-principles results for the intrachain magnetic interaction between Ni and Ir atoms. (a) Energy as a function of the angle between the magnetic moments of nearest-neighbor atoms. Blue squares are the energy calculated from DFT, and yellow circles are the energy obtained from the fitted anisotropic exchange model (AEM). (b) Same as in (a), but yellow circles are the energy obtained from the fitted model with anisotropic exchange and SIA on the Ni ion. (c) The angle that the Ir and Ni magnetic moments make with the [001] axis as a function of the angle between the magnetic moments of nearest-neighbor atoms.

in ϕ_{Ir} and ϕ_{Ni} as a function of $\phi_{\mathrm{Ni\text{-}Ir}}$. The only ferromagnetic state ($\phi_{\mathrm{Ni\text{-}Ir}} = 0$) is observed when $\phi_{\mathrm{Ir}} = \phi_{\mathrm{Ni}} = 90^\circ$, consistent with the previous observation that we could stabilize FM only if the moments are in the x-y plane [Fig. 3(b)]. Similarly, ferrimagnetic order ($\phi_{\mathrm{Ni\text{-}Ir}} = 180^\circ$) is observed only for $\phi_{\mathrm{Ir}} = 180^\circ$ and $\phi_{\mathrm{Ni}} = 0^\circ$, i.e., only when the moments are along $\mp\hat{z}$ [Fig. 3(a)]. The intermediate data points in Fig. 4 correspond to intermediate states where the moments have their z components ordered ferrimagnetically while the x components are ordered ferromagnetically [Fig. 3(d)]. Replacing the anisotropic interaction with an isotropic Heisenberg interaction and instead using the SIA to explain the Ising behavior would result in intermediate states with antialigned moments tilted away from the high-symmetry axes, such as those shown in Fig. 3(c). However, we never observed an intermediate state like this in Sr_3NiIrO_6, supporting the view that the interactions between the Ni and Ir ions are strongly anisotropic.

Fitting the energy values to the anisotropic exchange model, we get $J_\parallel = 19.0$ meV$/\mu_B^2$ and $J_\perp = -8.4$ meV$/\mu_B^2$. This simple model already fits the data quite well and gives the yellow data points in Fig. 4(a). The discrepancy between the first-principles results and the model is due to both the numerical error and the presence of a nonzero SIA. Introducing SIA to the anisotropic exchange model makes a small additional improvement in the agreement between the DFT result and the model fit, as shown in Fig. 4(b).

This is not the first study which uses an anisotropic exchange model for a compound with the K_4CdCl_6 structure, however this study extracts the exchange parameters $J_\perp$ and $J_\parallel$ from first principles and microscopically justifies them for this compound. This is also a prediction of opposite signs for $J_\perp$ and $J_\parallel$. Yin *et al.* have employed and microscopically justified a similar model to explain the magnetic anisotropy and magnon spectrum of Sr_3CuIrO_6 [13,34]. Also, both Toth *et al.* [21] and Lefrancois *et al.* used [20] a similar model to explain their experimental observations of magnon spectra of Sr_3NiIrO_6. The connection between the magnetic anisotropy and exchange interactions were apparent in the results of Gordon *et al.* [26], who determined that the FM order is more stable when the spins are aligned in the x-y plane, but their approach focused on the spin, not the pseudospin, of the Ir ion, and did not permit the construction of a simple magnetic Hamiltonian.

We have intentionally refrained from introducing a SIA term into our model to emphasize that the physics of Sr_3NiIrO_6 *can* be explained without it. A large SIA term is not physically justified in this compound: in a cubic environment Ni^{2+} has two e_g holes, and therefore no orbital angular momentum, and the $J_{\mathrm{eff}} = 1/2$ states of Ir are SU(2) symmetric and therefore are not supposed to have any SIA. The trigonal crystal field necessarily breaks this simple picture, but there is no apparent reason why the trigonal field in this material should be strong enough to give rise to a record-breaking coercive field as well as a very large magnon gap. The anisotropic exchange interaction, on the other hand, leads to a magnetic anisotropy energy that is the same order of magnitude as the magnetic exchange itself, and can be used to explain the large observed coercive field. The SIA is allowed by symmetry, and hence is definitely nonzero. However, our physical model, along with the first-principles calculations, show that it is not necessary to explain the experimental observations or the dominant source of anisotropy in Sr_3NiIrO_6. In other words, the *minimal* model sufficient to explain all the experimental and theoretical observations does not require a SIA term, even though adding SIA improves the quality of the fit to the DFT energies [Fig. 4(b)]. It is also possible to obtain an acceptable fit using a model with isotropic Heisenberg exchange and SIA; however, such a model does not explain the theoretically observed magnetic configurations, and is not well motivated. (See the Supplemental Material for further discussion of different possible models and their fit to the DFT energies [28].)

IV. MAGNONS

Magnons are commonly used to probe the nature of magnetic interactions. There are both inelastic neutron scattering

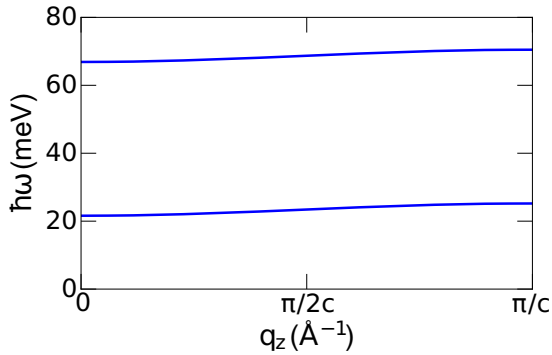

FIG. 5. Magnon spectra of Sr_3NiIrO_6 for wave vectors along the [001] direction in the magnetically ordered phase, obtained from the anisotropic exchange model.

(INS) and resonant inelastic x-ray scattering (RIXS) experiments that probed the magnon spectrum of Sr_3NiIrO_6 [20,21]. Even though each method is sensitive to only one of the two magnon branches in this compound, together they present a coherent picture: One of the branches has a width of ∼10 meV, and is around ∼35 meV. The other branch, dominated by Ir, is at ∼90 meV, and is almost dispersionless. These observations of a large magnon splitting and gap, much larger than the bandwidth, have previously been explained by a combination of anisotropic exchange, SIA, and Dzyaloshinskii-Moriya interactions [20,21]. Here we calculate the magnon spectrum of Sr_3NiIrO_6 using only the anisotropic exchange model with parameters from first principles to show that a model without SIA is sufficient to explain the large gap in the magnon spectrum.

We present the magnon spectra in Fig. 5 [28]. Our results correctly reproduce a large gap both between the two magnon branches and between the lower branch and the zero-energy axis. The quantitative agreement is not perfect, but his can be possibly fixed by fine-tuning the U parameters.

The sign of $J_\perp$ does not enter into the energy expression for the magnons, so the magnon spectra do not provide any evidence for the sign difference between $J_\parallel$ and $J_\perp$. However, there is a crucial effect of the radically anisotropic exchange: The characters (in-phase vs out-of-phase) of the acoustic and optical modes at the zone center are flipped: the lower energy magnon branch has an oscillation pattern like in Fig. 3(d), and not like in Fig. 3(c). As a result, the inelastic neutron-scattering cross sections of these magnons are also flipped: While a precise calculation of the cross sections for an inelastic neutron-scattering experiment is beyond the scope of this study, in the Supplemental Material [28] we provide a simple calculation that shows how the relative magnitudes of the magnon creation cross sections of the two branches depend on the sign and not just the magnitude of $J_\perp$. In other words, the relative intensities of the two branches carry information about the anisotropy in the exchange coupling, and experimental measurement of these intensities can provide the smoking gun evidence in support of the radically anisotropic exchange model. So far, the only neutron-scattering study on this compound [21] could not observe the higher energy branch, and as a result there are no data to verify our prediction.

V. CONCLUSIONS

The nearest-neighbor magnetic interaction in the chain compound Sr_3NiIrO_6 is not an isotropic Heisenberg exchange, but is rather radically anisotropic: The different components of magnetic moments are coupled with opposite signs. This explains the observations of both the strong Ising-type behavior and the large magnon gap without a large, physically unjustified SIA, thus resolving the mystery of the large coercivity observed in this compound. The magnon frequencies do not contain a feature that can differentiate between the SIA and anisotropic exchange, but our model has a signature in the magnon creation cross sections. An experiment that can quantify these cross sections can conclusively differentiate between the radically anisotropic exchange and SIA.

ACKNOWLEDGMENT

This work was supported by NSF DMREF Grant No. DMR-1629059.

[1] W. Witczak-Krempa, G. Chen, Y. B. Kim, and L. Balents, Correlated quantum phenomena in the strong spin-orbit regime, Annu. Rev. Condens. Matter Phys. **5**, 57 (2014).

[2] J. G. Rau, E. K.-H. Lee, and H.-Y. Kee, Spin-orbit physics giving rise to novel phases in correlated systems: Iridates and related materials, Annu. Rev. Condens. Matter Phys. **7**, 195 (2016).

[3] G. Khaliullin, Orbital order and fluctuations in mott insulators, Prog. Theor. Phys. Suppl. **160**, 155 (2005).

[4] M. Hermanns, I. Kimchi, and J. Knolle, Physics of the kitaev model: fractionalization, dynamical correlations, and material connections, Annu. Rev. Condens. Matter Phys. **9**, 17 (2018).

[5] M. Ležaić and N. A. Spaldin, High-temperature multiferroicity and strong magnetocrystalline anisotropy in 3*d*-5*d* double perovskites, Phys. Rev. B **83**, 024410 (2011).

[6] K. Rolfs, S. Tóth, E. Pomjakushina, D. T. Adroja, D. Khalyavin, and K. Conder, Incommensurate magnetic order in a quasicubic structure of the double-perovskite compound Sr_2NiIrO_6, Phys. Rev. B **95**, 140403 (2017).

[7] O. Erten, O. N. Meetei, A. Mukherjee, M. Randeria, N. Trivedi, and P. Woodward, Theory of Half-Metallic Ferrimagnetism in Double Perovskites, Phys. Rev. Lett. **107**, 257201 (2011).

[8] R. Morrow, R. Mishra, O. D. Restrepo, M. R. Ball, W. Windl, S. Wurmehl, U. Stockert, B. Buüchner, and P. M. Woodward, Independent ordering of two interpenetrating magnetic sublattices in the double perovskite Sr_2CoOsO_6, J. Am. Chem. Soc. **135**, 18824 (2013).

[9] H. Das, P. Sanyal, T. Saha-Dasgupta, and D. D. Sarma, Origin of magnetism and trend in T_c in CR-based double perovskites:

Interplay of two driving mechanisms, Phys. Rev. B **83**, 104418 (2011).

[10] R. Morrow, K. Samanta, T. Saha Dasgupta, J. Xiong, J. W. Freeland, D. Haskel, and P. M. Woodward, Magnetism in Ca_2CoOsO_6 and Ca_2NiOsO_6: Unraveling the mystery of superexchange interactions between 3d and 5d ions, Chem. Mater. **28**, 3666 (2016).

[11] G. Bergerhoff and O. Schmitz-Dumont, Die kristallstruktur des kaliumhexachlorocadmats (ii), Z. Anorg. Allg. Chem. **284**, 10 (1956).

[12] H. Wu, T. Burnus, Z. Hu, C. Martin, A. Maignan, J. C. Cezar, A. Tanaka, N. B. Brookes, D. I. Khomskii, and L. H. Tjeng, Ising Magnetism and Ferroelectricity in Ca_3CoMnO_6, Phys. Rev. Lett. **102**, 026404 (2009).

[13] W.-G. Yin, X. Liu, A. M. Tsvelik, M. P. M. Dean, M. H. Upton, J. Kim, D. Casa, A. Said, T. Gog, T. F. Qi, G. Cao, and J. P. Hill, Ferromagnetic Exchange Anisotropy from Antiferromagnetic Superexchange in the Mixed 3*d*-5*d* Transition-Metal Compound Sr_3CuIrO_6, Phys. Rev. Lett. **111**, 057202 (2013).

[14] E. V. Sampathkumaran and A. Niazi, Superparamagnetic-like ac susceptibility behavior in the partially disordered antiferromagnetic compound Ca_3CoRhO_6, Phys. Rev. B **65**, 180401 (2002).

[15] S. Niitaka, K. Yoshimura, K. Kosuge, M. Nishi, and K. Kakurai, Partially Disordered Antiferromagnetic Phase in Ca_3CoRhO_6, Phys. Rev. Lett. **87**, 177202 (2001).

[16] D. Mikhailova, C. Y. Kuo, P Reichel, A. A. Tsirlin, A. Efimenko, M. Rotter, M. Schmidt, Z. Hu, T. W. Pi, L. Y. Jang *et al.*, Structure, magnetism, and valence states of cobalt and platinum in quasi-one-dimensional oxides A_3CoPtO_6 with A= Ca, Sr, J. Phys. Chem. C **118**, 5463 (2014).

[17] T. N. Nguyen, D. M. Giaquinta, and H.-C. Zur Loye, Synthesis of the new one-dimensional compound Sr_3NiPtO_6: Structure and magnetic properties, Chem. Mater. **6**, 1642 (1994).

[18] T. N. Nguyen and H.-C. Zur Loye, A family of one-dimensional oxides: Sr_3MIrO_6 (M= Ni, Cu, Zn): Structure and magnetic properties, J. Solid State Chem. **117**, 300 (1995).

[19] J. Singleton, J. W. Kim, C. V. Topping, A. Hansen, E.-D. Mun, S. Chikara, I. Lakis, S. Ghannadzadeh, P. Goddard, X. Luo, Y. S. Oh, S.-W. Cheong, and V. S. Zapf, Magnetic properties of Sr_3NiIrO_6 and Sr_3CoIrO_6: Magnetic hysteresis with coercive fields of up to 55 T, Phys. Rev. B **94**, 224408 (2016).

[20] E. Lefrançois, A.-M. Pradipto, M. Moretti Sala, L. C. Chapon, V. Simonet, S. Picozzi, P. Lejay, S. Petit, and R. Ballou, Anisotropic interactions opposing magnetocrystalline anisotropy in Sr_3NiIrO_6, Phys. Rev. B **93**, 224401 (2016).

[21] S. Toth, W. Wu, D. T. Adroja, S. Rayaprol, and E. V. Sampathkumaran, Frustrated ising chains on the triangular lattice in Sr_3NiIrO_6, Phys. Rev. B **93**, 174422 (2016).

[22] G. V. Vajenine, R. Hoffmann, and H.-C. zur Loye, The electronic structures and magnetic properties of one-dimensional ABO_6 chains in Sr_3ABO_6 (A= Co, Ni; B= Pt, Ir) and two-dimensional MO_3 sheets in $InMO_3$ (M= Fe, Mn), Chem. Phys. **204**, 469 (1996).

[23] G. R. Zhang, X. L. Zhang, T. Jia, Z. Zeng, and H. Q. Lin, Intrachain antiferromagnetic interaction and mott state induced by spin-orbit coupling in Sr_3NiIrO_6, J. Appl. Phys. **107**, 09E120 (2010).

[24] S. Sarkar, S. Kanungo, and T. Saha-Dasgupta, Ab initio study of low-dimensional quantum spin systems Sr_3NiPtO_6, Sr_3CuPtO_6, and Sr_3NiIrO_6, Phys. Rev. B **82**, 235122 (2010).

[25] X. Ou and H. Wu, Impact of spin-orbit coupling on the magnetism of Sr_3MIrO_6 (M= Ni, Co), Sci. Rep. **4**, 4609 (2014).

[26] E. E. Gordon, H. Xiang, J. Köhler, and M.-H. Whangbo, Spin orientations of the spin-half Ir^{4+} ions in Sr_3NiIrO_6, Sr_2IrO_4, and Na_2IrO_3: Density functional, perturbation theory, and madelung potential analyses, J. Chem. Phys. **144**, 114706 (2016).

[27] E. Lefrançois, L. C. Chapon, V. Simonet, P. Lejay, D. Khalyavin, S. Rayaprol, E. V. Sampathkumaran, R. Ballou, and D. T. Adroja, Magnetic order in the frustrated ising-like chain compound Sr_3NiIrO_6, Phys. Rev. B **90**, 014408 (2014).

[28] See Supplemental Material at http://link.aps.org/supplemental/10.1103/PhysRevB.98.134432, which includes Refs. [35–46], for further discussion of different possible models and their fit to the DFT energies, details of the crystal and electronic structure, calculation of the magnon spectrum, details of the Wannier tight binding model, and the U dependence of magnetic interactions.

[29] G. Jackeli and G. Khaliullin, Mott Insulators in the Strong Spin-Orbit Coupling Limit: From Heisenberg to a Quantum Compass and Kitaev Models, Phys. Rev. Lett. **102**, 017205 (2009).

[30] J. Kim, A. H. Said, D. Casa, M. H. Upton, T. Gog, M. Daghofer, G. Jackeli, J. van den Brink, G. Khaliullin, and B. J. Kim, Large Spin-Wave Energy Gap in the Bilayer Iridate $Sr_3Ir_2O_7$: Evidence for Enhanced Dipolar Interactions Near the Mott Metal-Insulator Transition, Phys. Rev. Lett. **109**, 157402 (2012).

[31] J. B. Goodenough, *Magnetism and the Chemical Bond*, Interscience Monographs on Chemistry: Inorganic Chemistry Section (Interscience, New York, 1963).

[32] N. Marzari, A. A. Mostofi, J. R. Yates, I. Souza, and D. Vanderbilt, Maximally localized wannier functions: Theory and applications, Rev. Mod. Phys. **84**, 1419 (2012).

[33] N. Marzari and D. Vanderbilt, Maximally localized generalized wannier functions for composite energy bands, Phys. Rev. B **56**, 12847 (1997).

[34] X. Liu, V. M Katukuri, L. Hozoi, W.-G. Yin, M. Dean, M. H. Upton, J. Kim, D. Casa, A. Said, T. Gog *et al.*, Testing the Validity of the Strong Spin-Orbit-Coupling Limit for Octahedrally Coordinated Iridate Compounds in a Model System Sr_3CuIrO_6, Phys. Rev. Lett. **109**, 157401 (2012).

[35] G. Kresse and J. Furthmuller, Efficiency of ab-initio total energy calculations for metals and semiconductors using a plane-wave basis set, Comput. Mater. Sci. **6**, 15 (1996).

[36] G. Kresse and J. Furthmüller, Efficient iterative schemes for *ab initio* total-energy calculations using a plane-wave basis set, Phys. Rev. B **54**, 11169 (1996).

[37] P. E. Blöchl, Projector augmented-wave method, Phys. Rev. B **50**, 17953 (1994).

[38] G. Kresse and D. Joubert, From ultrasoft pseudopotentials to the projector augmented-wave method, Phys. Rev. B **59**, 1758 (1999).

[39] J. P. Perdew, A. Ruzsinszky, G. I. Csonka, O. A. Vydrov, G. E. Scuseria, L. A. Constantin, X. Zhou, and K. Burke, Restoring the Density-Gradient Expansion for Exchange in Solids and Surfaces, Phys. Rev. Lett. **100**, 136406 (2008).

[40] S. L. Dudarev, G. A. Botton, S. Y. Savrasov, C. J. Humphreys, and A. P. Sutton, Electron-energy-loss spectra and the structural

stability of nickel oxide: An LSDA+U study, Phys. Rev. B **57**, 1505 (1998).

[41] R. Hoffmann, J. M. Howell, and A. R. Rossi, Bicapped tetrahedral, trigonal prismatic, and octahedral alternatives in main and transition group six-coordination, J. Am. Chem. Soc. **98**, 2484 (1976).

[42] M. I. Aroyo, J. M. Perez-Mato, C. Capillas, E. Kroumova, S. Ivantchev, G. Madariaga, A. Kirov, and H. Wondratschek, Bilbao crystallographic server: I. databases and crystallographic computing programs, Z. Kristallogr. **221**, 15 (2006).

[43] P. Fazekas, *Lecture Notes on Electron Correlation and Magnetism* (World Scientific, Singapore, 1999), Vol. 5.

[44] S. W. Lovesey, *Theory of Neutron Scattering from Condensed Matter*, International Series of Monographs on Physics No. 2 (Clarendon Press, Oxford, 1986).

[45] P. Liu, S. Khmelevskyi, B. Kim, M. Marsman, D. Li, X.-Q. Chen, D. D. Sarma, G. Kresse, and C. Franchini, Anisotropic magnetic couplings and structure-driven canted to collinear transitions in Sr_2IrO_4 by magnetically constrained noncollinear DFT, Phys. Rev. B **92**, 054428 (2015).

[46] I. Solovyev, N. Hamada, and K. Terakura, Crucial Role of the Lattice Distortion in the Magnetism of $LaMnO_3$, Phys. Rev. Lett. **76**, 4825 (1996).